Simultaneous observations of reconnection pulses at Cluster and their effects on the cusp aurora observed at the Chinese Yellow River Station

Q.-H. Zhang,[1] M. W. Dunlop,[2] M. Lockwood,[2] R.-Y. Liu,[1] H.-Q. Hu,[1] H.-G. Yang,[1] Z.-J. Hu,[1] Y. V. Bogdanova,[3] C. Shen,[4] B.-C. Zhang,[1] D.-S. Han,[1] S.-L. Liu,[1] I. W. McCrea,[2] and M. Lester[5]

Received 1 April 2010; revised 17 June 2010; accepted 23 June 2010; published 20 October 2010.

[1] While the Cluster spacecraft were located near the high-latitude magnetopause, between 1010 and 1040 UT on 16 January 2004, three typical flux transfer event (FTE) signatures were observed. During this interval, simultaneous and conjugated all-sky camera measurements, recorded at Yellow River Station, Svalbard, are available at 630.0 and 557.7 nm that show poleward-moving auroral forms (PMAFs), consistent with magnetic reconnection at the dayside magnetopause. Simultaneous FTEs seen at the magnetopause mainly move northward, but having duskward (eastward) and tailward velocity components, roughly consistent with the observed direction of motion of the PMAFs in all-sky images. Between the PMAFs meridional keograms, extracted from the all-sky images, show intervals of lower intensity aurora which migrate equatorward just before the PMAFs intensify. This is strong evidence for an equatorward eroding and poleward moving open-closed boundary associated with a variable magnetopause reconnection rate under variable IMF conditions. From the durations of the PMAFs, we infer that the evolution time of FTEs is 5–11 minutes from its origin on the magnetopause to its addition to the polar cap.

Citation: Zhang, Q.-H., et al. (2010), Simultaneous observations of reconnection pulses at Cluster and their effects on the cusp aurora observed at the Chinese Yellow River Station, *J. Geophys. Res.*, *115*, A10237, doi:10.1029/2010JA015526.

1. Introduction

[2] Magnetic reconnection is the dominant process that causes energy and momentum transfer from the solar wind to the magnetosphere. The process was first discussed in terms of a steady dynamic process by *Dungey* [1961], but subsequently *Haerendel et al.* [1978] and *Russell and Elphic* [1978] interpreted signatures on the magnetopause as intermittent and spatially limited reconnection. The magnetic signatures arising from the passage of bundles of reconnected magnetic flux produced by transient reconnection as they moved nearby a spacecraft location were named flux transfer events (FTEs) by *Russell and Elphic* [1978]. The most typical magnetic signature is a bipolar oscillation in the magnetic field component normal to the magnetopause. Subsequent studies addressed the mixing of magnetosheath and magnetospheric plasma populations caused by reconnection [e.g., *Daly et al.*, 1981; *Thomsen et al.*, 1987; *Farrugia et al.*, 1988], accelerated ion flows [e.g., *Paschmann et al.*, 1982], and their larger occurrence rate during periods of southward interplanetary magnetic field (IMF) [e.g., *Berchem and Russell*, 1984; *Lockwood and Smith*, 1992]. These features are largely common to newly reconnected field lines produced by both steady and pulsed reconnection.

[3] Because of the limitation of single-point spacecraft measurements at the magnetopause, it has been difficult to determine the spatial distribution and motion of FTEs. One can gain some information by comparing in situ space observations at separate locations, but determining the full extent of events is only possible by looking at the response of the ionosphere and the geomagnetic field seen at the ground. Part of this response reflects the global flow system (driven by reconnection in the tail as well as at the magnetopause), and part is directly linked to the bursty and intermittent nature of local dayside reconnection. *Lockwood et al.* [1989, 1993] showed that transient dayside auroral events were associated with co-located bursts of ionospheric flow and that both were consistent with reconnection rate pulses.

[4] The first direct association of magnetopause FTE signatures and the ionospheric signatures was made by *Elphic et al.* [1990] who demonstrated that ionospheric flow

[1]SOA Key Laboratory for Polar Science, Polar Research Institute of China, Shanghai, China.
[2]SSTD, Rutherford-Appleton Laboratory, Chilton, Didcot, Oxfordshire, UK.
[3]Mullard Space Science Laboratory, University College London, Dorking, Surrey, UK.
[4]CSSAR, Chinese Academy of Sciences, Beijing, China.
[5]Department of Physics and Astronomy, University of Leicester, Leicester, UK.

0148-0227/10/2010JA015526

bursts measured by European Incoherent Scatter (EISCAT) followed FTE events recorded by the ISEE-1 and -2 satellites. *Neudegg et al.* [1999] showed magnetically conjugate measurements of an FTE (by the Equator-S satellite) and its associated ionospheric flow burst (detected by the Super Dual Auroral Radar Network (SuperDARN) radars [*Greenwald et al.*, 1995; *Chisham et al.*, 2007]). The changes in the global aurora (in visible light and UV) in the vicinity of the reconnection footprint for the same event were subsequently discussed by *Neudegg et al.* [2001].

[5] Recently, observations by Cluster [*Escoubet et al.*, 2001] of FTEs have been combined with a variety of ground-based instruments [e.g., *Wild et al.*, 2001, 2003, 2007], and with other spacecraft located at the magnetopause [*Dunlop et al.*, 2005, 2008; *Wang et al.*, 2007]. Statistically, the distribution of the repetition rates of pulsed ionospheric flows and poleward moving auroral forms is in agreement with the distribution of FTE occurrence at the magnetopause [*Lockwood and Wild*, 1993; *McWilliams et al.*, 2000; *Frey et al.*, 2002, 2003], although the data sets are typically restricted from the point of view of one-to-one measurements. Some questions still remain. For example, the much-cited theory of *Cowley and Lockwood* [1992], which has been very successful in explaining many observed features of newly opened flux as it is appended to the polar cap (including cusp auroral particle dispersions, transient flow bursts, PMAFs, cusp current signatures), predicts that, because of the induction effect of changing magnetospheric magnetic field, it is the addition of newly open flux that drives dayside ionospheric convection, not the existence of open flux. However, induction effects also mean that initially the newly open-field lines are straightening rather than driving convection [*Lockwood and Morley*, 2004]. Hence the variation of the voltage contribution during the evolution of a newly open flux tube (FTE), from its generation at the magnetopause to its disappearance in the global magnetospheric convection [*Amm et al.*, 2005], is not well known, especially considering the variability in the location of reconnection onset and the development of the reconnection rates. The Cluster observations and the subsequent coordination with Double Star have given the opportunity to probe more directly the relationship between multiple locations on the magnetopause and ground signatures [*Liu et al.*, 2005a].

[6] In this paper, we present the features of three large, typical FTEs which were simultaneously observed by the four Cluster spacecraft at the high-latitude magnetopause, and by cameras observing the dayside aurora. Using the Cluster observations, we calculated the velocity and the size of the flux tubes. Using simultaneous measurements, the motion of FTEs is shown to be roughly consistent with the observed PMAF motion in all-sky images observed at Yellow River Station, Svalbard. We study the motion of the inferred open-closed boundary and infer the evolution time of the FTEs, and discuss the ionospheric convection observed by the SuperDARN radars, which are driven by the FTEs measured by Cluster.

2. Instrumentation

[7] The Cluster spacecraft [*Escoubet et al.*, 2001] were launched in pairs in July and August 2000 into elliptical, polar orbits with a perigee of 4 R_E, an apogee of 19.6 R_E, and identical orbital periods of 57 h. Data with 0.2 s resolution from the fluxgate magnetometer (FGM) [*Balogh et al.*, 1997] on the four Cluster spacecraft and with 4 s resolution from the Plasma Electron and Current Experiment (PEACE) [*Johnstone et al.*, 1997] on the Cluster spacecraft 2 are used in this study.

[8] An optical observation system [*Liu et al.*, 2005b; *Hu et al.*, 2009] was installed at the Chinese Yellow River Station (YRS), at Ny-Ålesund, Svalbard in November 2003. This optical system consists of three all-sky cameras supplied with the narrow-band filters centered at 427.8, 557.7, and 630.0 nm. The emission intensities for each line and the corresponding emission height can be used to deduce the energy flux of the precipitating electrons. Furthermore, the magnetospheric sources of precipitating electrons can be traced back along the magnetic field line, if allowance is made for the motion of the field line during the particle flight times.

[9] The SuperDARN radars [*Greenwald et al.*, 1995; *Chisham et al.*, 2007] measure the line-of-sight (LOS) velocity of the ionospheric plasma in 16 adjacent beam directions separated by 3.24° in azimuth. A full scan, completed in 2 minutes, thus covers 52° in azimuth and over 3,000 km in range with a resolution of 45 km. They provide a way to monitor two-dimensional convection in the high-latitude ionosphere on a global scale. We present the ionospheric convection patterns with the map potential plots, derived by using the technique of *Ruohoniemi and Baker* [1998], applied to the data from nine of the Northern Hemisphere radars during the interval of interest.

[10] The ACE satellite is in a halo orbit around the L1 Lagrange point and monitors the upstream solar wind and IMF conditions. The ACE spacecraft is located at about (231.4, −40.0, 22.3) R_E in GSM coordinates around 0930 UT on 16 January 2004. Solar wind data with 64 s resolution from the Solar Wind Experiment [*McComas et al.*, 1998] and IMF data with 16 s resolution from the Magnetometer instrument [*Smith et al.*, 1998] onboard the ACE spacecraft are used in this study.

3. Observations and Results

[11] Figure 1 shows the orbit of Cluster spacecraft in the *X-Y*, *Y-Z*, and *X-Z* planes in GSM coordinates, together with the observed magnetic field vectors (in green), on 16 January 2004. The plot shows the configuration of the Cluster spacecraft array was a tetrahedron (scaled up in size in Figure 1 by a factor of 20). Figure 1 also shows the best-fit model magnetopause (MP) for the prevailing solar wind conditions: cuts in the *X-Y*, *Y-Z*, and *X-Z* planes are presented in Figure 1a, 1b, and 1c, respectively. Model geomagnetic field lines are also shown for the projection into the *X-Z* plane in Figure 1c. The ionospheric footprints of Cluster 1 are plotted on the map of the Northern Hemisphere presented in Figure 1d. The field lines and ionospheric footprints of Cluster 1 are drawn using the *Tsyganenko* '01 model [*Tsyganenko et al.*, 2002a, 2002b] of the magnetospheric field for the average prevailing values of the input parameters: the solar wind dynamic pressure, $P_{dyn} = 4.18$ nPa, IMF $B_Y = -4.22$ nT, IMF $B_Z = -3.11$ nT, and the geomagnetic index $Dst = -30$ nT. Although the model does not

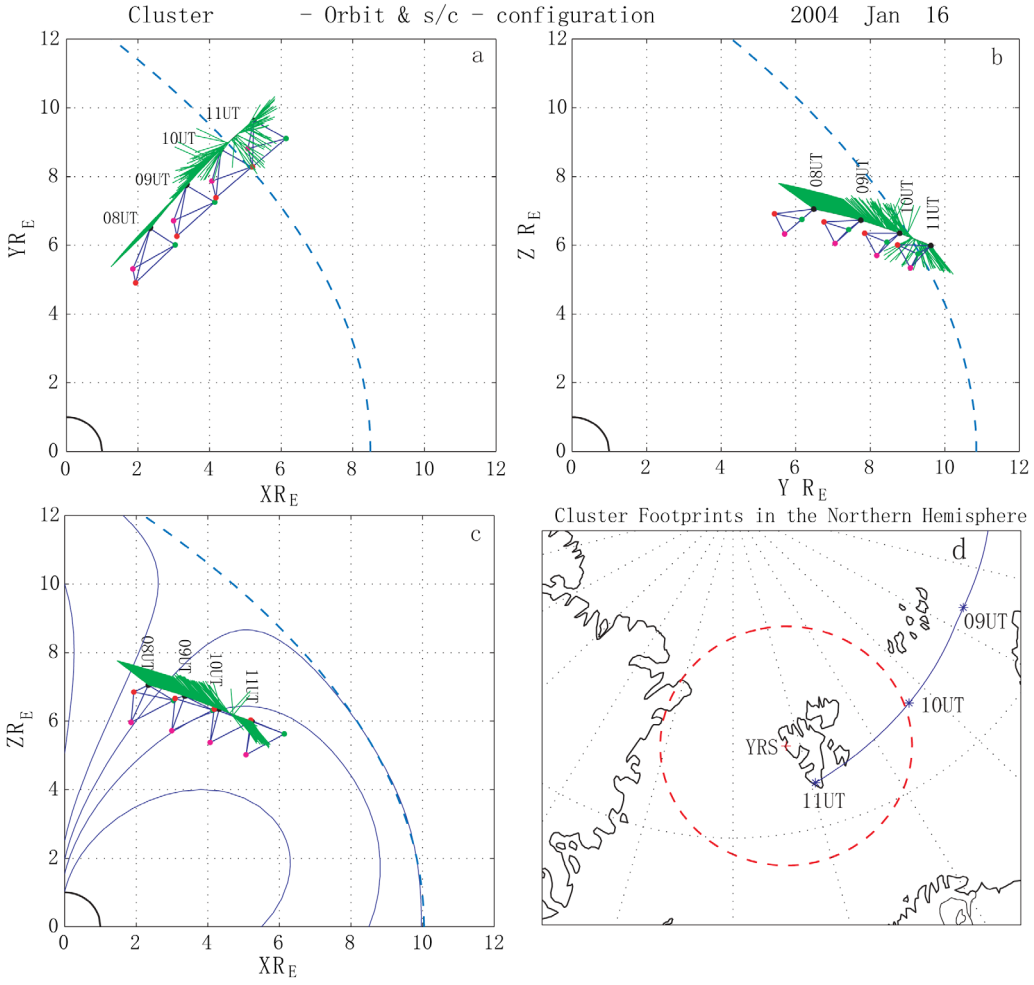

Figure 1. Cluster spacecraft tracks in the (a) *X*-*Y*, (b) *Y*-*Z*, and (c) *X*-*Z* planes in GSM coordinates, together with magnetic field vectors (projected onto the plane in question and shown in green), on 16 January 2004. The orbit also shows the configuration of the Cluster spacecraft array as a tetrahedron (size scaled up by a factor of 20). Cuts through the best-fitting model MP are shown as blue dashed lines for the *X*-*Y*, *Y*-*Z*, and *X*-*Z* planes and model geomagnetic field lines are also shown for the projection into the *X*-*Z* plane in Figure 1c. (d) The ionospheric footprints of Cluster 1 spacecraft are plotted on the map of Northern Hemisphere. The field lines and ionospheric footprints of Cluster 1 are drawn from the Tsyganenko '01 model with the average input parameters: solar wind dynamic pressure, P_{dyn} = 4.18 nPa, IMF B_Y = −4.22 nT, IMF B_Z = −3.11 nT, and *Dst* = −30 nT. The field of view of the 630.0 nm all-sky imager at Chinese Yellow River Station is presented as red dashed circle in Figure 1d, for an assumed emission altitude of 250 km.

estimate the field near the magnetopause well (the magnitude of the deviation between the model field at Cluster and the measured field is around ±10 nT before about 1025 UT), such differences make only small differences to the field line mapping and the footprints are roughly reliable before 1025 UT. The field of view of the 630.0 nm all-sky imager at Chinese Yellow River Station at Ny-Ålesund, Svalbard is presented as a dashed circle in Figure 1d, for an assumed emission altitude of 250 km. The Cluster spacecraft cross through the cusp and/or the boundary layer, eventually crossing the dusk flank magnetopause into the magnetosheath at about 1025 UT. During the interval of interest, the predicted footprints of Cluster cross the southern part of the field of view of the all-sky imager (see Figure 1d) from east to west. In fact, the footprints should disappear after about 1025 UT, because the spacecraft exited through the magnetopause around this time. Note that because the model does not estimate the field near the magnetopause well, there are uncertainties in the end point of the footprint locus.

3.1. Upstream Solar Wind and IMF Conditions

[12] Figure 2 presents an overview of the solar wind and IMF conditions measured by the ACE satellite. Parameters shown are the IMF components (in the GSM frame of reference) of B_X, B_Y, B_Z, the IMF clock angle, the solar wind plasma number density, the solar wind speed, and the solar wind dynamic pressure. The data have all been lagged by 40.4 min which is the estimated propagation delay from the spacecraft to the magnetopause: this time delay is calculated from the best fit to the magnetosheath data (particularly the

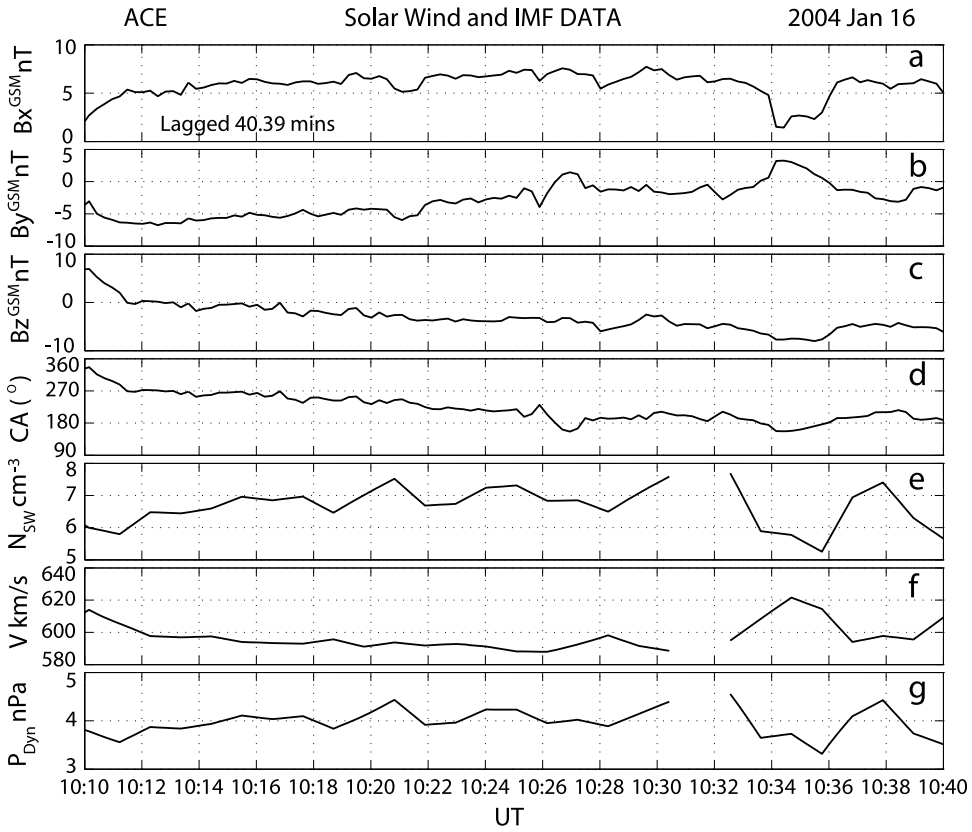

Figure 2. An overview of the solar wind and IMF conditions measured by the ACE satellite. Parameters shown are: the GSM IMF components (a) B_X; (b) B_Y; (c) B_Z; (d) the IMF clock angle, CA; (e) the solar wind plasma number density, N; (f) the solar wind speed, V; and (g) the solar wind dynamic pressure, P_{dyn}.

IMF clock angle which is largely conserved on crossing the bow shock) observed by Cluster after 1025 UT. During the whole interval, the IMF B_Z component was mainly negative with some short positive excursions at the beginning of the interval, varying between −8.5 and 2.6 nT (see Figure 2c), while the B_Y component was negative before about 1025 UT (lagged time) and after 1036 UT (lagged time), and varied around zero during the middle interval (see Figure 1b). The IMF clock angle (defined as positive for rotation from the $+Z$ direction toward $+Y$) mainly varied between 135° and 302° during this period (see Figure 2d). The solar wind density increased from 6 to 8 cm^{-3} before about 1030 UT and varied between 5 and 8 cm^{-3} after about 1033 UT with a data gap between them at 1030:30–1032:30 UT (see Figure 2e), whilst the solar wind velocity varied between 587 and 622 km/s (see Figure 2f), resulting in a prevailing solar wind dynamic pressure in the range 3.3–4.6 nPa (see Figure 2g).

3.2. Cluster Observations

[13] Figure 3 plots the magnetic field data from all four Cluster spacecraft, together with the IMF clock angle (lagged by 40.4 minutes) from the ACE satellite for the interval of interest. In Figure 3a the lagged interplanetary clock angle is compared to the same angle seen by Cluster 1. It can be seen that after Cluster 1 emerges into the magnetosheath (at the vertical magenta dot-dashed line) the two traces agree closely. In Figures 3b–3e, the data are expressed in local boundary normal coordinates (LMN), which are found by performing the minimum variance analysis (MVA), with eigenvalues $[\lambda_1, \lambda_2, \lambda_3] = [848.4, 192.7, 34.3]$, on the local magnetopause crossing of Cluster 1 between about 1016 and 1030 UT to obtain the mean boundary normal **n**, where **l** = (−0.43, −0.26, 0.87), **m** = (−0.55, 0.83, −0.02) and **n** = (0.71, 0.49, 0.50) in GSM coordinates. This boundary normal direction is typical for the location of Cluster on the magnetopause. The IMF clock angle shows a slow change, but for most of the interval it is predominantly westward and southward. During the interval, two magnetospheric and one magnetosheath bipolar signatures in boundary-normal component B_N were detected (see Figure 3c) and the vertical red dot-dash lines (at 1015, 1019, and 1033 UT) highlight that the total field strength $|B|$ (see Figure 3d) shows a peak at the centers of each of these bipolar B_{N} signatures. These typical FTE signatures are seen by all four Cluster spacecraft and show signatures of the so-called "standard polarity" events [*Russell and Elphic*, 1978], with the B_{N} component being positive then negative, consistent with a northward moving flux tube from a low-latitude reconnection site passing over the Cluster satellites which, as shown in Figure 1, are at middle latitudes in the Northern Hemisphere. The time difference of these signatures is very small, and the perturbations in the B_{N} component and magnitude of the magnetic field are much greater than the background magnetosheath fluctua-

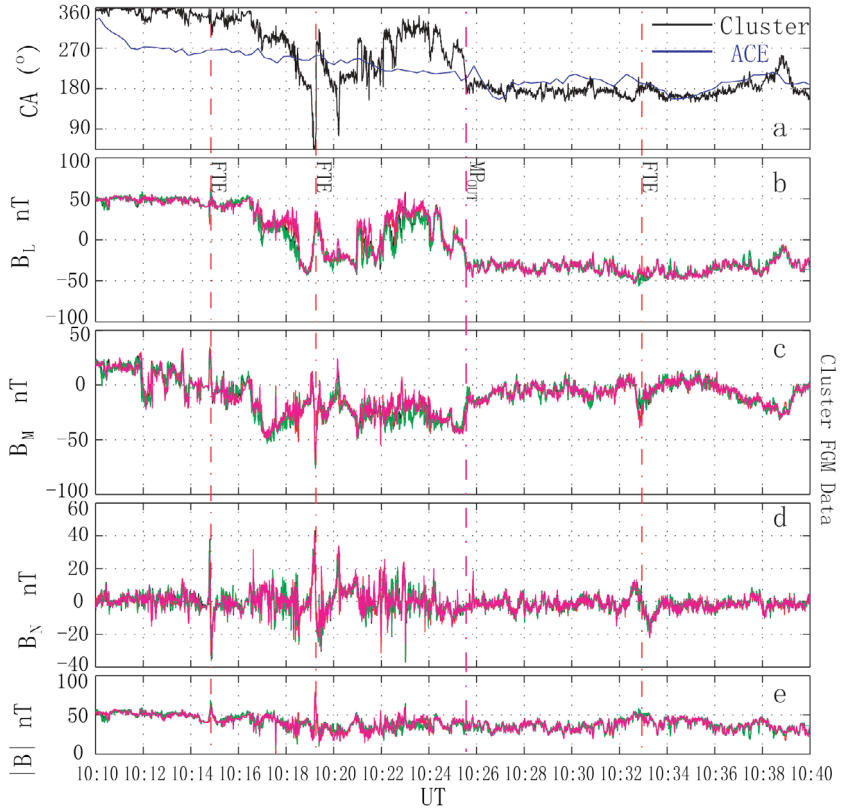

Figure 3. (a) The magnetic field and IMF clock angle as measured by the ACE satellite (lagged by 40.39 minutes) and the corresponding value seen by the Cluster 1 spacecraft. (b)–(e) Overview of the Cluster FGM magnetic field measurement, presented in the boundary-normal (LMN) coordinate system between 1010 and 1040 UT on 16 January 2004. The vertical red dot-dashed lines highlight the three typical FTEs at 1014:48, 1019:17, and 1032:57 UT, and the magnetopause crossing by Cluster 1 is given by the magenta dot-dashed vertical line.

tions, which indicate that the signatures are FTEs and not surface waves [*Song et al.*, 1994]. The variations in magnitude between the positive and negative peaks in the B_N signature of the magnetospheric FTEs are much larger than the corresponding one in the magnetosheath FTEs. Inspection of the solar wind conditions shows that the IMF clock angle (Figure 3a) exhibited a varying southward IMF component (clock angles 135° to 270°), favoring low-latitude reconnection.

[14] Unfortunately, since there are no plasma data from Cluster before about 1020 UT, we cannot study the mixing of magnetosheath and magnetospheric plasma populations on the newly reconnected field lines for the first two FTEs. There is good data set, however, from one of the four spacecraft (Cluster 2) after 1020 UT, which provides us the opportunity to carry out a detailed analysis for the last FTE, when the spacecraft were in the magnetosheath.

[15] Figures 4a and 4b present the detail of the B_N component (same as Figure 3c) and $|B|$ of the magnetic field data, respectively, for a short interval around the magnetosheath FTE. The other panels show energy-time electron spectrograms of spin-averaged, differential electron energy flux in the (c) anti-parallel, (d) perpendicular, and (e) parallel directions from the HEEA and LEEA sensors of the PEACE electron instrument on Cluster 2. Note that in Figure 4 there are a few white stripes which correspond to intervals with missing data from half of a spacecraft spin measurements. The FTE is delineated by two red dot-dash lines with the magnetopause crossing shown by the purple dot-dashed vertical line. From Figure 4, we can find that Cluster 2 crossed the open field line regions and cusp or boundary layer between about 1020 and 1025 UT and encountered the magnetopause at about 1025 UT. The spacecraft were subsequently in the magnetosheath. Around about 1033 UT, the Cluster spacecraft sampled a typical magnetosheath FTE signature with a clear mixing of magnetosheath and magnetospheric plasma populations near the event core. The reappearance of magnetospheric electrons (at energies above about 300 eV) in the FTE event is clearest in the anti-parallel direction which is consistent with outflowing magnetospheric electrons for this Northern Hemisphere event. They indicate that the satellite has cut the core of the open flux tube of the event and has not just remotely sensed the event through its draping effect on the magnetosheath field. Note, however, that at between 1032:58 and 1033:10 UT fluxes are also weakly increased in the parallel direction, revealing a mirror point, probably associated with the field threading the bow shock. Careful inspection reveals that the returning parallel magnetospheric electrons are nested inside the outgoing ones: this shows that the satellite moves from newly reconnected field lines on the first edge of the event core onto field lines that have been open

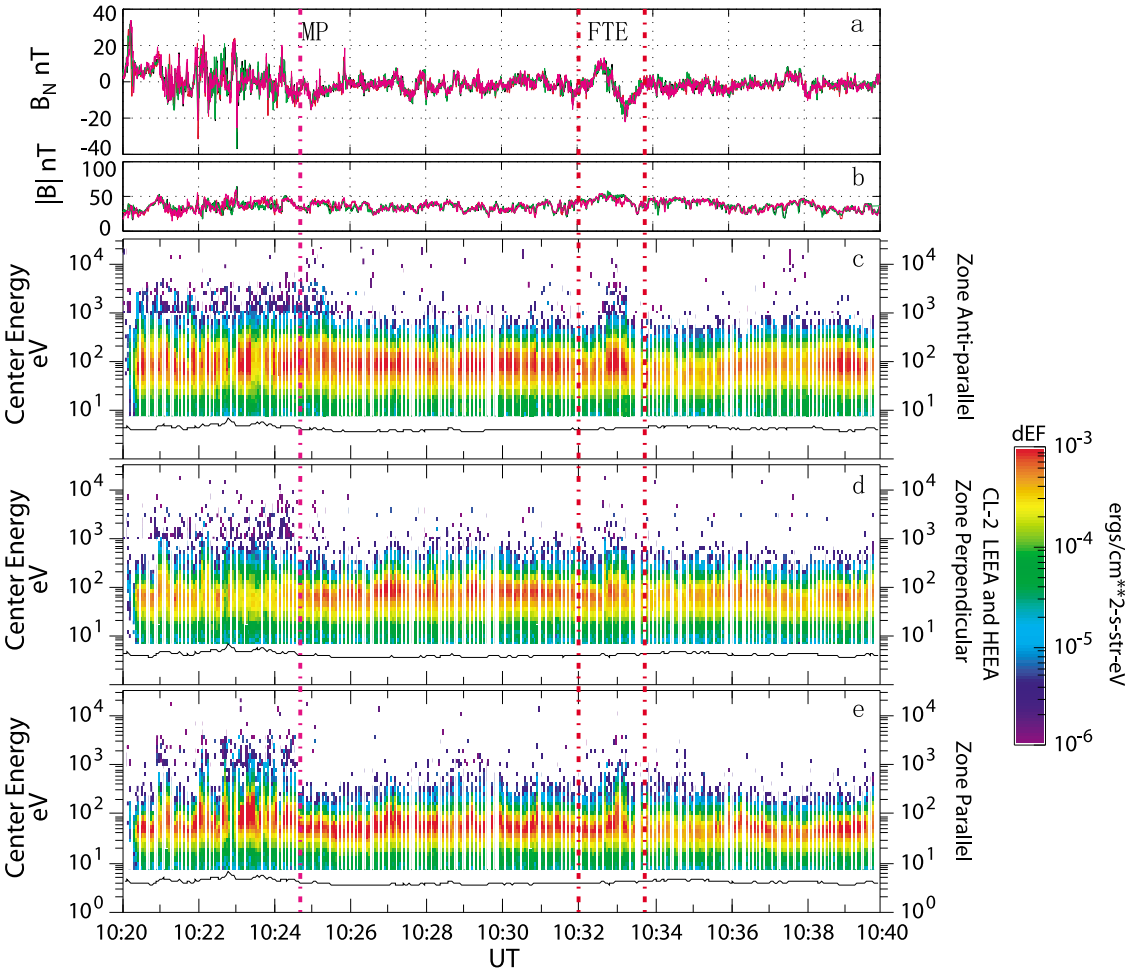

Figure 4. Detailed plot for the interval around the third (magnetosheath) FTE. (a) the magnetic field boundary normal component B_N (as in Figure 3c) and (b) the field magnitude. The energy-time electron spectrograms of spin-averaged, differential electron energy flux in the (c) anti-parallel, (d) perpendicular, and (e) parallel directions from the HEEA and LEEA sensor of PEACE on Cluster 2.

slightly longer at the center of the event core (so that electrons have had time to mirror and return to the spacecraft), before moving back on the more recently reconnected flux tubes on the trailing edge of the event core. This is consistent with the two-dimensional (2-D) reconnection pulse model [*Saunders et al.*, 1983; *Southwood et al.*, 1988], where the model explains the bulge as the effect of a pulse of enhanced reconnection rate at an *X*-line whose length is not specified.

[16] Since the magnetometers on all four spacecraft sample these FTEs, we may apply a number of four-spacecraft techniques, including timing analysis [*Russell et al.*, 1983; *Harvey*, 1998; *Dunlop et al.*, 2001] and Spatio-Temporal Difference [*Shi et al.*, 2006], to calculate the motion and scale of the FTEs as they move over the tetrahedral spacecraft configuration. The results from the two techniques are almost identical. For the 1015 UT event, the speed and the direction (in GSM coordinates) of the motion is Un = 324.67 km/s, $\hat{n}_v$ = (−0.10, 0.27, 0.96), confirming the northward motion, but having a duskward (eastward) component as expected for the geometry and prevailing IMF B_Y component. The velocity and the duration of the whole bipolar signature (23 s), give an estimated (minimum) FTE dimension in the direction of travel of 1.17 R_E. For the 1019 UT event, Un = 298.45 km/s, $\hat{n}_v$= (−0.38, 0.14, 0.91), giving a strong northward component, but still eastward, and the corresponding FTE size is estimated as 1.12 R_E. For the 1033 UT event, Un = 237.90 km/s, $\hat{n}_v$ = (−0.45, 0.19, 0.87), giving a strong northward component and again still eastward. The corresponding FTE size was 3.02 R_E (larger than the former one and lasting 81 s as a result). These motions are consistent with the evolution of Northern Hemisphere flux tubes moving northward as they are dragged across the magnetopause, under the influence of magnetosheath flow and the magnetic curvature force and are sampled en-route by Cluster.

3.3. The Cusp Aurora Seen at Yellow River Station

[17] To investigate the signatures of these FTEs in the cusp aurora, images from the all-sky cameras at the Chinese Yellow River Station have been employed. Figure 5 presents the keograms of temporal variation of emission intensities along the magnetic meridian at (a) 557.7 nm and (b) 630.0 nm between 1010 and 1040 UT, respectively, on 16 January 2004. The red dot-dash vertical lines present the core time of the FTEs shown in Figure 3. From Figure 5b,

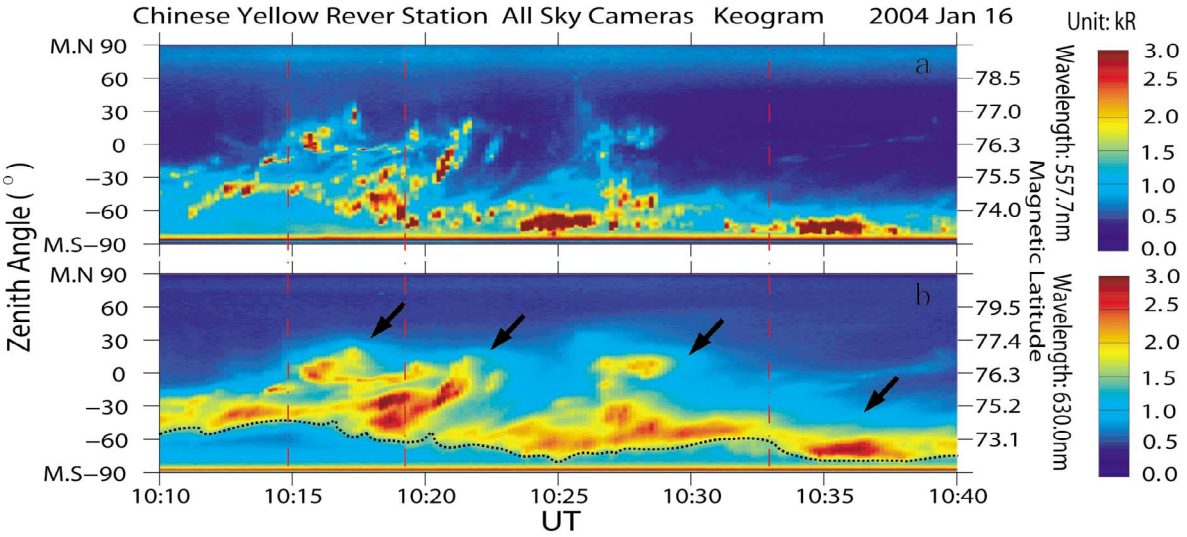

Figure 5. Keograms of temporal variation of emission intensities along the magnetic meridian at (a) 557.7 nm and (b) 630.0 nm between 1010 and 1040 UT, respectively, on 16 January 2004 as observed from the Chinese Yellow River Station. The corresponding magnetic latitude to the zenith angle are shown at the right *Y*-axis, which are different in Figures 5a and 5b because the images are projected from 150 km for 557.7 nm and 250 km for 630.0 nm, respectively.

we can find the equatorward edge of the brightening 630.0 nm aurora highlighted by the black dashed line, which is generally accepted as lying close to the open-closed field line boundary (OCB) [e.g., *Sandholt et al.*, 1990; *Lockwood et al.*, 1993; *Milan et al.*, 1999]. In the absence of reconnection this electron edge is at the OCB. But the presence of reconnection generates a velocity across the OCB (in its own rest frame), with the consequence that the most energetic electrons arrive somewhat poleward of the OCB. The electron edge moved equatorward from about −54° to −82° in the zenith angle of the all sky cameras, which corresponds to 73.7° to 71.6° in magnetic latitude (see Figure 5b), due to the IMF B_Z southward turning at the beginning of the interval. At the time of the second (third) event, the electron edge erodes equatorward from about 1017 UT (1020 UT), just ahead of the FTE signature time, and then relaxes back again from about 1019 to 1022 UT (1025 to 1032 UT). That this is not seen in association with the first event is attributed to the fact that the boundary is still in motion because of the swing to the more southward IMF. As the boundary migrates back poleward, we see an intensification of the 630.0 nm aurora and the 557.7 nm aurora. The poleward motion for the last event is difficult to see as by this time the cusp aurora is close to the southern limit of the field of view and large motions in distance cause only small changes in observation zenith angle.

[18] It has become widely accepted that poleward moving auroral forms (PMAFs) are the auroral signatures of FTEs [e.g., *Sandholt et al.*, 1986, 1990; *Davis and Lockwood*, 1996]. In this interval, there are four clear PMAFs, with some substructures inside them, in the keograms at 630.0 and 557.7 nm (highlighted by black arrows in Figure 5b), and clear intensity gaps are present around 1011, 1017, 1020, and 1033 UT with poleward OCB motion occurring thereafter. These effects show a clear illustration of the ionospheric response of pulse reconnection as shown in Figure 6. Figure 6 is a simplified and improved version of Figure 1b in the paper by *Davis and Lockwood* [1996] for a single event. Davis and Lockwood described how the OCB erodes equatorward immediately after a pulse of reconnection occurs at the low-latitude magnetopause, only starting to relax back when the reconnection slows or stops. It is during the poleward return that the poleward velocity V_x is enhanced, and this cannot happen until the Alfvén wave from the reconnection site has arrived in the ionosphere. The incoming magnetosheath electrons that we have used to identify the electron edge in Figure 5 (from the equatorward edge of the 630.0 nm aurora) are sub-Alfvénic, and so the Alfvén wave lies between the OCB and the electron edge. For these events, intensity gaps or weaker intensity regions before the PMAFs show strong evidence for equatorward eroding, and the poleward moving OCB shows strong evidence for a variable reconnection rate under variable IMF conditions.

[19] In Figure 6, the Alfvén wave propagates into the polar ionosphere from the reconnection *X*-line after about 1 minute, and electrons and ions precipitate into ionosphere after about 2 and 4 minutes, respectively. This means that there is about a 2 minute delay from reconnection *X*-line to the subsequent 630.0 nm response in the polar ionosphere. The time constant for the flows to cease is of the order of 10 min [*Lockwood and Wild*, 1993; *Zhang et al.*, 2008], but depends on a number of parameters, including the ionospheric and thermospheric densities (which determine the frictional force on the moving thermal ionospheric ions exerted by the neutral atoms).

[20] In Figure 5b we identify, for each PMAF, a prior interval when the intensity of 630 nm emission is weaker, and these "gaps" are accompanied by an equatorward motion of the equatorward edge of the emission. The time

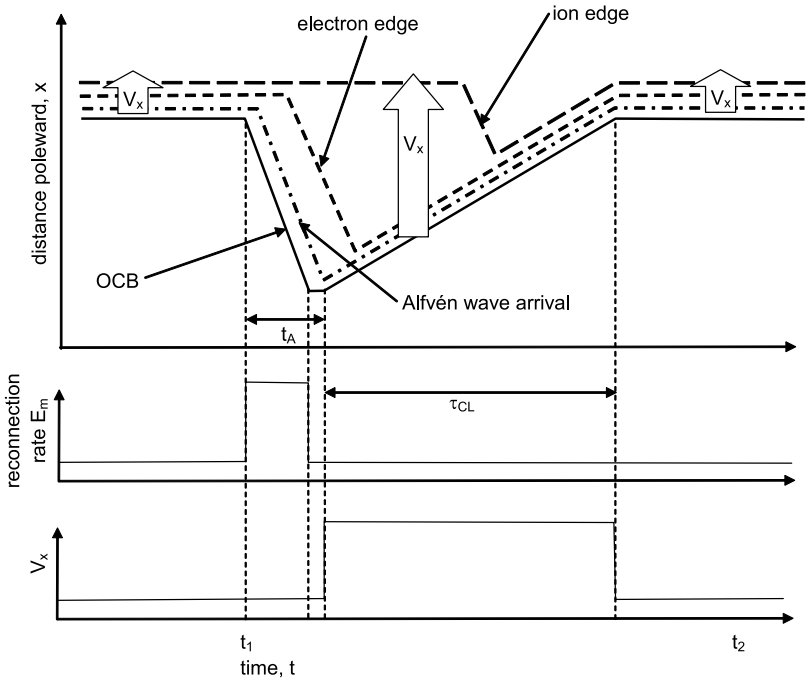

Figure 6. A sketch of response of various boundaries in the ionosphere to a pulse of magnetopause reconnection rate (E_m) between times t_1 and t_2, over a background level. The flight time of an Alfvén wave from the magnetopause reconnection site to the ionosphere is t_A and the poleward ionospheric velocity, V_x, is only increased t_A after the reconnection pulse onset. The Cowley-Lockwood response time for the polar cap to come to equilibrium with the new amount of open flux is τ_{CL}. In reality, both the rise and fall of V_x will not be instantaneous as shown here. The boundaries shown are: the open-closed boundary; the latitude at which the Alfvén wave launched at the reconnection site arrives in the ionosphere, the electron edge, and the ion edge.

delays between the beginning of the gaps and the enhancement of the PMAFs are about 1.7, 2.1, 2.5, and 1.8 minutes for the four events. These delays are reasonably consistent with the above estimate of 2 minutes, and this implies that the distance from the ionosphere to the reconnection site has not changed radically between events. The timing of the PMAFs strongly suggests that they are associated with the three FTEs observed by Cluster and shown in Figure 3, but we note that for the third PMAF event no clear FTE signature was seen by Cluster. This is almost certainly because a classical FTE signature is not produced when the spacecraft is close to the magnetopause, such that the center of a flux tube passes over the spacecraft. One can observe oscillating signatures in the magnetic field B_N component (see Figure 4a) when the spacecraft is very close to the magnetopause (often called B_N activity". However, it is difficult to determine how this signature relates to the FTE signature seen further away from the current sheet center because of the complicated distributions and motions of the current sheets and boundary layers. We note that in the original study by *Elphic et al.* [1990], one event was seen in ground-based radar and cameras but was similarly missed by spacecraft close to the magnetopause (but the missing event was, as in the present case, replaced by B_N activity).

[21] Figure 7 shows selected 10 second integrated all-sky images recorded during this auroral sequence, as seen by the 630.0 all-sky camera at Chinese Yellow River Station. The LOS intensities have been mapped onto a geographic grid by a constant and single emission altitude of 250 km. Note that this procedure means that rays with extended range of emission altitude appear as elongated structures which radiate from the magnetic zenith. From Figure 7, we can see that there is a weak and thin auroral band with some bright patches inside (labeled *C*) at almost constant *L* values, well to the south of Svalbard during this whole auroral sequence. Whilst, a second aurora form, identifiable from the keograms as a PMAF (labeled *A*), has arisen from southwest of the field of view at about 1009:22 UT. It intensified and moved northeast before fading after about 1014:20 UT (it has disappeared by about 1020:47 UT). This PMAF has moved about 450 km from southwest to northeast of Svalbard and lasted about 11 minutes. This suggests that the FTE footprint moved in the northeast direction with a velocity of about 680 m/s and took about 11 minutes between its origin on magnetopause and its addition to the polar cap. At 1018:28 UT, another PMAF (labeled *B*) arose at the south of Svalbard. Subsequently, PMAF *B* developed and brightened, began fading after 1022:27 UT, and disappeared at about 1023:26 UT. This PMAF has moved 150 km in northeast with a speed of about 500 m/s and an evolution time of 5 minutes. Note that the equatorward edge of the brightening region has suddenly moved southwest (southeast) associated with PMAF *A* (*B*) at about 1009:22 UT (1018:28 UT). This confirms the

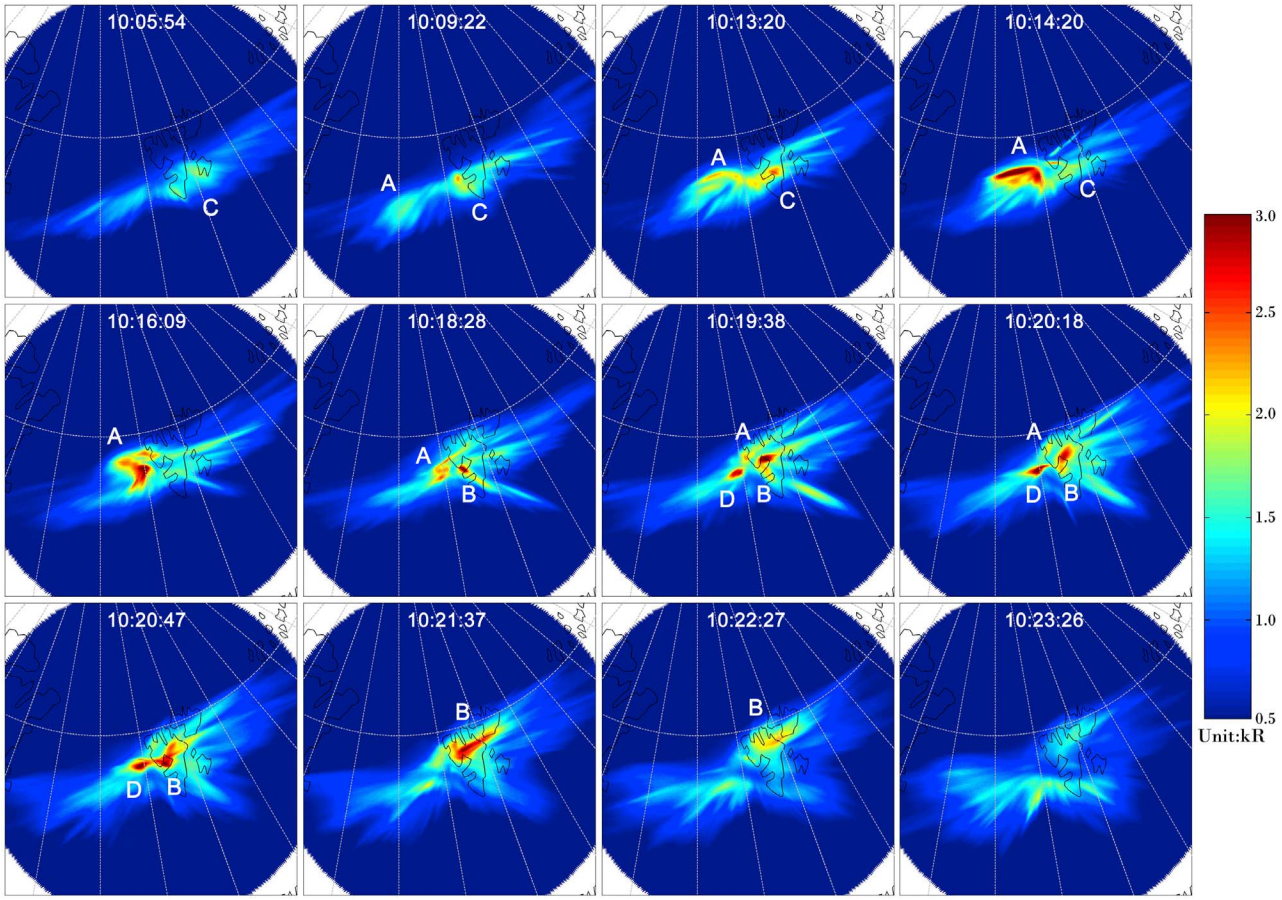

Figure 7. Sequence of 10 second integrated images observed by the 630.0 all-sky imager during 1005:54–1023:26 UT on 16 January 2004. Each all-sky image is projected to an altitude of 250 km and shown on the background of a grid representing geographic coordinates. Svalbard is in the center and Greenland east coast is to the left in each frame.

boundary motions expected from the predictions of *Davis and Lockwood* [1996] (see Figure 6) and seen in the keogram data (Figure 5).

4. Discussion

[22] It is difficult to monitor the one-to-one correspondence of ionospheric features to magnetopause FTEs since there is a large spatial separation between the two and different measurement constraints. Furthermore, although the footprint of the reconnection site may be in the imager field of view, the magnetopause satellites are removed from the *X*-line, and there will be a propagation delay before they reach the satellites which would be absent for the ground-based imager data if the reconnection site footprint is within the field of view. We note here, however, that the ionospheric flow direction is consistent with the motion of FTEs at the magnetopause [*Zhang et al.*, 2008]. *Zhang et al.* [2008] found that the flux tube motion, both measured and modeled from the inferred *X*-line, qualitatively matches the clear velocity enhancements and the flow directions in ionospheric convections at each location in both hemispheres, measured simultaneously by the SuperDARN radar network. The large field of view of SuperDARN allows us to see better one-to-one correspondence with magnetopause signatures. For the events studied in the present paper, the Cluster footprints were mainly located in the overlapped region between the fields of view of the two CUTLASS radars of the SuperDARN network and of the all-sky cameras at Yellow River Station. We have also checked the SuperDARN observations which show that there are only clear velocity enhancements in the region above Svalbard in the field of view of CUTLASS radars. Figure 8 shows successive flow maps for the Northern Hemisphere from CUTLASS for 10:12 to 1038 UT. Grayed concentric circles indicate lines of constant magnetic latitude in 10° increments. Noon is located at the top of each pattern. The IMF in the IMF *Y*-*Z* plane is shown as a red vector, under which the time delay from ACE to the ionosphere is presented in parentheses. (Typically this is around 44 min, i.e., 41 min of which is the propagation time from ACE to Cluster, mainly in the magnetosheath, and 3 min to account for the field-aligned travel time to the ionosphere.) The field of view of the CUTLASS radars (HAN and PYK) is presented as fans in Figure 8a. The red circle, which mainly located in the field of view of the CUTLASS, highlights the region of velocity enhancement, as indicated by increased numbers of red drift vectors. Unfortunately, the data from CUTLASS Iceland radar (PYK) are absent throughout the period under study, so the statistical convection model [*Ruohoniemi and*

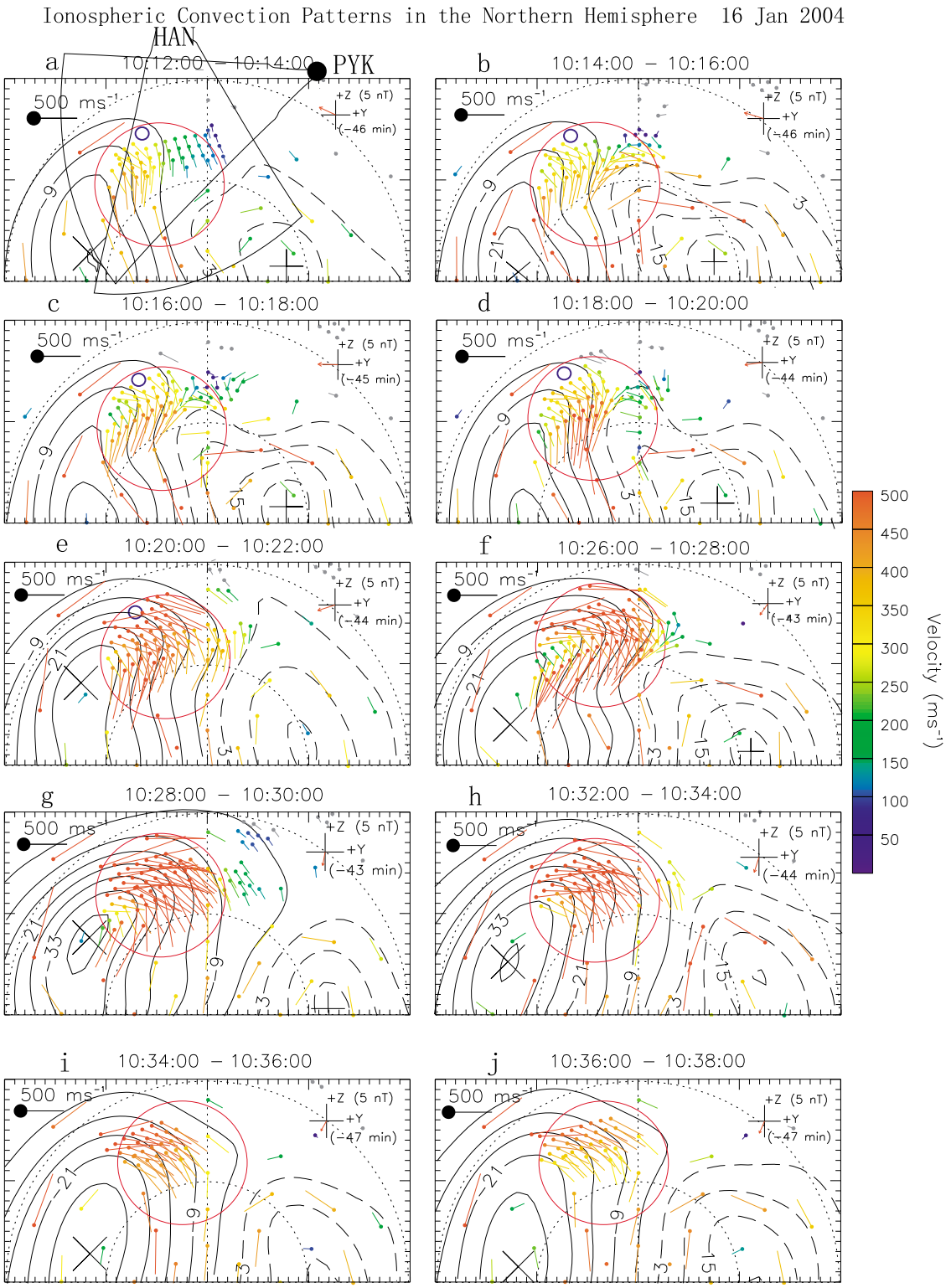

Figure 8. Streamlines and vectors of the ionospheric flows during 1012 and 1038 UT derived from the Northern Hemispheric SuperDARN velocity measurements shown on geomagnetic grids, obtained from the "map potential" algorithm. The field of view of the CUTLASS radars (HAN and PYK) are presented as a fan in Figure 8a, respectively. The direction and magnitude of the lagged IMF are indicated by the red vector at the right-hand upper corner of each map. The small open blue circle is the footprint of the Cluster spacecraft.

Greenwald, 1996], which in the absence of data is used by the map potential algorithm to close the spherical harmonics expansion of the potential [*Ruohoniemi and Baker*, 1998], played an important role in determining the convection maps.

[23] In Figure 8, there are clear velocity enhancements at the near-noon, high-latitude section on the afternoon cell from 1018 to 1036 UT (Figures 8d–8i), which correspond to the response of the first three events in Figure 5b. These are seen at Cluster near 1015, 1019, and 1026. Note that the timing difference between the Cluster and CUTLASS observations would be $(t_f - t_m)$, where t_m is the time for the FTE to propagate over the magnetopause from the reconnection site to the satellite, and t_f is the time for the flows to exceed a detectable threshold following reconnection. The small blue open circles in Figures 8a–8e are the footprint of the Cluster spacecraft 1 at the time of the center of each scan. Near these positions, the drift vectors in the flow cell are strongly northward. There is a clear enhancement in flow speeds between 1020 and 1028 UT, and the vector directions are consistent with the directions of the motion of the PMAF *A* and *B* in Figure 7 and of the motion of the 1015 and 1019 UT FTEs across the magnetopause observed by Cluster. The drift vectors turn dawnward and northward between 1028 and 1036 UT, also corresponding to the third events in Figure 5b. We also note that the Cluster position lies on magnetospheric field lines computed from the *Tsyganenko* '01 model, rather than at the boundary, and therefore that the computed footprints lie slightly equatorward of the likely true locations. These points suggest that at least the first two FTEs have motions which reflect the likely flow directions at the respective positions of their footprints. The convection cell pattern infers a relatively direct global context for the evolution of the sampled FTEs.

5. Conclusions

[24] We have presented features of three typical FTEs which are confirmed by simultaneous and conjugate observations by the Cluster spacecraft tetrahedron at the high-latitude magnetopause and the all-sky cameras on Svalbard measuring the aurora brightening. Using the Cluster four-spacecraft observations, we have calculated the velocity and the size of the inferred, reconnected flux tubes as they pass by the Cluster spacecraft. These are shown to mainly move northward, but having duskward (eastward) and tailward velocity components. The simultaneous measurements show that the FTEs motion is roughly consistent with the observed PMAFs moving direction in all-sky images seen at Yellow River Station, Svalbard. The clear intensity gaps or weaker regions in the keograms of all-sky images before PMAFs show strong evidence for equatorward erosion followed by poleward motion which is expected for a variable reconnection rate. The time durations of the PMAF *A* and *B* infer that the evolution time of FTEs is about 5 and 11 minutes from its origin on magnetopause before the precipitation is shut off by its addition to the polar cap.

[25] **Acknowledgments.** This work is supported by the National Natural Science Foundation of China (NSFC grant No. 40890164, 40604020, 41031064) and National Science and Technology Pillar Program of China (Grant No. 2006BAB18B06). M. W. Dunlop is partly supported by Chinese Academy of Sciences (CAS) visiting Professorship for senior international scientists (Grant No. 2009S1-54). M. Lester is supported by STFC grant ST/H002480/1. We acknowledge the NASA CDA Web site for supplying us the solar wind and IMF data from the ACE spacecraft. We also thank the Cluster FGM Operations Team and FGM PI, Dr. Lucek, for the magnetic field data, and the Cluster PEACE Operations Team and PEACE PI, Dr A. N. Fazakerley, for the electron spectrometer data.

[26] Masaki Fujimoto thanks the reviewers for their assistance in evaluating this paper.

References

Amm, O., E. F. Donovan, H. Frey, M. Lester, R. Nakamura, J. A. Wild, A. Aikio, M. Dunlop, K. Kauristie, A. Marchaudon, I. W. McCrea, H. J. Opgenoorth, and A. Strømme (2005), Coordinated studies of the geospace environment using Cluster, satellite and ground-based data: an interim review, *Ann. Geophys.*, *23*, 2129–2170.

Balogh, A., et al. (1997), The Cluster magnetic field investigation, *Space Sci. Rev.*, *79*, 65–91.

Berchem, J., and C. T. Russell (1984), Flux transfer events on the magnetopause: Spatial distribution and controlling factors, *J. Geophys. Res.*, *89*(A8), 6689–6703.

Cowley, S. W. H., and M. Lockwood (1992), Excitation and decay of solar-wind driven flows in the magnetosphere-ionosphere system, *Ann. Geophys.*, *10*, 103–115.

Chisham, G., M. Lester, S. E. Milan, M. P. Freeman, W. A. Bristow, A. Grocott, K. A. MacWilliams, J. M. Ruohoniemi, T. K. Yeoman, P. Dyson, R. A. Greenwald, T. Kikuchi, M. Pinnock, J. Rash, N. Sato, G. Sofko, J.-P. Villain, and A. D. M. Walker (2007), A decade of the Super Dual Auroral Radar Network (SuperDARN): Scientific achievements, new techniques and future directions, *Surv. Geophys.*, *28*, 33–109.

Daly, P. W., D. J. Williams, C. T. Russell, and E. Keppler (1981), Particle signature of magnetic flux transfer events at the magnetopause, *J. Geophys. Res.*, *86*(A3), 1628–1632.

Davis, C. J., and M. Lockwood (1996), Predicted signatures of pulsed reconnection in ESR data, *Ann. Geophys.*, *14*, 1246–1256.

Dungey, J. W. (1961), Interplanetary magnetic field and the auroral zones, *Phys. Rev. Lett.*, *6*, 47–48.

Dunlop, M. W., et al. (2001), Cluster observes the Earth's magnetopause: Coordinated four-point magnetic field measurements, *Ann. Geophys.*, *19*, 1449–1460.

Dunlop, M. W., M. G. G. T. Taylor, J. A. Davies, C. J. Owen, F. Pitout, A. N. Fazakerley, Z. Pu, H. Laakso, Y. V. Bogdanova, Q.-G. Zong, C. Shen, K. Nykyri, B. Lavraud, S. E. Milan, T. D. Phan, H. Rème, C. P. Escoubet, C. M. Carr, P. Cargill, M. Lockwood, and B. Sonnerup (2005), Coordinated Cluster/Double Star observations of dayside reconnection signatures, *Ann. Geophys.*, *23*, 2867–2875.

Dunlop, M. W., M. G. G. T. Taylor, Y. V. Bogdanova, C. Shen, F. Pitout, Z. Pu, J. A. Davies, Q.-H. Zhang, J. Wang, B. Lavraud, A. N. Fazakerley, A. Walsh, C. J. Owen, H. Laakso, Q.-G. Zong, Z.-X. Liu, C. P. Escoubet, C. M. Carr, and H. Rème (2008), Energization in the electron boundary layer: Cluster/Double star observations at high and low latitude, *J. Geophys. Res.*, *113*, A07S19, doi:10.1029/2007JA012788.

Elphic, R. C., M. Lockwood, S. W. H. Cowley, and P. E. Sandholt (1990), Flux transfer events at the magnetopause and in the ionosphere, *Geophys. Res. Lett.*, *17*(12), 2241–2244.

Escoubet, C. P., M. Fehringer, and M. Goldstein (2001), Introduction: the Cluster mission, *Ann. Geophys.*, *19*, 1197–1200.

Farrugia, C. J., R. P. Rijnbeek, M. A. Saunders, D. J. Southwood, D. J. Rodgers, M. F. Smith, C. P. Chaloner, D. S. Hall, P. J. Christiansen, and L. J. C. Woolliscroft (1988), A multi-instrument study of flux transfer event structure, *J. Geophys. Res.*, *93*(A12), 14465–14477.

Frey, H. U., S. B. Mende, T. J. Immel, S. A. Fuselier, E. S. Claflin, J.-C. Gérard, and B. Hubert (2002), Proton aurora in the cusp, *J. Geophys. Res.*, *107*(A7), 1091, doi:10.1029/2001JA900161.

Frey, H. U., S. B. Mende, S. A. Fuselier, T. J. Immel, and N. Østgaard (2003), Proton aurora in the cusp during southward IMF, *J. Geophys. Res.*, *108*(A7), 1277, doi:10.1029/2003JA009861.

Greenwald, R. A., K. B. Baker, J. R. Dudeney, M. Pinnock, T. B. Jones, E. C. Thomas, J.-P. Villain, J.-C. Cerisier, C. Senior, C. Hanuise, R. D. Hunsucker, G. Sofko, J. Koehler, E. Nielsen, R. Pellinen, A. D. M. Walker, N. Sato, and H. Yamagishi (1995), DARN/SuperDARN: A global view of the dynamics of high-latitude convection, *Space Sci. Rev.*, *71*(1–4), 761–796.

Haerendel, G., G. Paschmann, N. Sckopke, H. Rosenbauer, and P. Hedgecock (1978), The frontside boundary layer of the magnetosphere and the problem of reconnection, *J. Geophys. Res.*, *83*(A7), 3195–3216.

Harvey, C. C. (1998), Spatial gradients and the volumetric tensor, in: *Analysis Methods for MultiSpacecraft Data*, ISSI Scientific Report

Series, EAS/ISSI, vol. 1, edited by G. Paschmann and P. W. Daly, pp. 307–322, Int. Space Sci. Inst., Bern.

Hu, Z.-J., H. Yang, D. Huang, T. Araki, N. Sato, M. Taguchi, E. Seran, H. Hu, R. Liu, B. Zhang, D. Han, Z. Chen, Q. Zhang, and S. Liu (2009), Synoptic distribution of dayside aurora: Multiple-wavelength all-sky observation at Yellow River Station in Ny-Ålesund, Svalbard, *J. Atmos. Sol. Terr. Phys.*, *71*(8–9), 794–804.

Johnstone, A. D., et al. (1997), Peace: A plasma electron and current experiment, *Space Sci. Rev.*, *79*, 351–398, doi:10.1023/A:1004938001388.

Liu, Z.-X., C. P. Escoubet, Z. Pu, H. Laakso, J. K. Shi, C. Shen, and M. Hapgood (2005a), The Double Star mission, *Ann. Geophys.*, *23*, 2707–2712.

Liu, R.-Y., Y.-H. Liu, Z.-H. Xu, H.-Q. Hu, H.-G. Yang, B.-C. Zhang, W.-Y. Xu, G.-X. Chen, J. Wu, W.-M. Zhen, D.-H. Huang, Z.-J. Hu, and Z.-X. Deng (2005b), The Chinese ground-based instrumentation in support of the combined Cluster/Double Star satellite measurements, *Ann. Geophys.*, *23*, 2943–2951.

Lockwood, M., and S. E. Morley (2004), A numerical model of the ionospheric signatures of time-varying magnetic reconnection: I. Ionospheric convection, *Ann. Geophys.*, *22*, 73–91.

Lockwood, M., and M. F. Smith (1992), The variation of reconnection rate at the dayside magnetopause and cusp ion precipitation, *J. Geophys. Res.*, *97*(A10), 14841–14847.

Lockwood, M., and M. N. Wild (1993), On the quasi-periodic nature of magnetopause flux transfer events, *J. Geophys. Res.*, *98*(A4), 5935–5940.

Lockwood, M., P. E. Sandholt, S. W. H. Cowley, and T. Oguti (1989), Interplanetary magnetic field control of dayside auroral activity and the transfer of momentum across the dayside magnetopause, *Planet. Space Sci.*, *37*, 1347–1365.

Lockwood, M., W. F. Denig, A. D. Farmer, V. N. Davda, S. W. H. Cowley, and H. Lühr (1993), Ionospheric signatures of pulsed magnetic reconnection at the Earth's magnetopause, *Nature*, *361*(6411), 424–428.

McComas, D. J., S. J. Bame, P. Barker, W. C. Feldman, J. L. Phillips, P. Riley, and J. W. Griffee (1998), Solar Wind Electron Proton Alpha Monitor (SWEPAM) for the Advanced Composition Explorer, *Space Sci. Rev.*, *86*, 563–612.

McWilliams, K. A., T. K. Yeoman, and G. Provan (2000), A statistical survey of dayside pulsed ionospheric flows as seen by the CUTLASS Finland HF radar, *Ann. Geophys.*, *18*, 445–453.

Milan, S. E., M. Lester, S. W. H. Cowley, J. Moen, P. E. Sandholt, and C. J. Owen (1999), Meridian-scanning photometer, coherent HF radar, and magnetometer observations of the cusp: a case study, *Ann. Geophys.*, *17*, 159–172.

Neudegg, D. A., T. K. Yeoman, S. W. H. Cowley, G. Provan, G. Haerendel, W. Baumjohann, U. Auster, K.-H. Fornacon, E. Georgescu, and C. J. Owen (1999), A flux transfer event observed at the magnetopause by the Equator-S spacecraft and in the ionosphere by the CUTLASS HF radar, *Ann. Geophys.*, *17*, 707–711.

Neudegg, D. A., S. W. H. Cowley, K. A. McWilliams, M. Lester, J. Sigwarth, G. Haerendel, W. Baumjohann, U. Auster, K.-H. Fornacon, and E. Georgescu (2001), The UV aurora and ionospheric flows during flux transfer events, *Ann. Geophys.*, *19*, 179–188.

Paschmann, G., G. Haerendel, I. Papamastorakis, N. Sckopke, S. Bame, J. Gosling, and C. Russell (1982), Plasma and magnetic field characteristics of magnetic flux transfer events, *J. Geophys. Res.*, *87*(A4), 2159–2168.

Ruohoniemi, J. M., and K. B. Baker (1998), Large-scale imaging of high-latitude convection with Super Dual Auroral Radar Network HF radar observations, *J. Geophys. Res.*, *103*(A9), 20797–20811.

Ruohoniemi, J. M., and R. A. Greenwald (1996), Statistical patterns of high-latitude convection obtained from the Goose Bay HF radar observations, *J. Geophys. Res.*, *101*(A10), 21743–21763.

Russell, C. T., and R. C. Elphic (1978), Initial ISEE magnetometer results: magnetopause observations, *Space Sci. Rev.*, *22*, 681–715.

Russell, C. T., M. M. Mellott, E. J. Smith, and J. H. King (1983), Multiple spacecraft observations of interplanetary shocks: Four spacecraft determination of shock normals, *J. Geophys. Res.*, *88*(A12), 4739–4748.

Sandholt, P., C. Deehr, A. Egeland, B. Lybekk, R. Viereck, and G. Romick (1986), Signatures in the dayside aurora of plasma transfer from the magnetosheath, *J. Geophys. Res.*, *91*(A9), 10063–10079.

Sandholt, P., M. Lockwood, T. Oguti, S. Cowley, K. Freeman, B. Lybekk, A. Egeland, and D. Willis (1990), Midday auroral breakup events and related energy and momentum transfer from the magnetosheath, *J. Geophys. Res.*, *95*(A2), 1039–1060.

Saunders, M. A., C. T. Russell, and N. Sckopke (1983), Recent ISEE observations of the magnetopause and low-latitude boundary layer: a review, *J. Geophys.*, *52*(3), 190–198.

Shi, Q. Q., C. Shen, M. W. Dunlop, Z. Y. Pu, Q.-G. Zong, Z. X. Liu, E. Lucek, and A. Balogh (2006), Motion of observed structures calculated from multi-point magnetic field measurements: Application to Cluster, *Geophys. Res. Lett.*, *33*, L08109, doi:10.1029/2005GL025073.

Smith, C. W., M. H. Acuna, L. F. Burlaga, J. L'Heureux, N. F. Ness, and J. Scheifele (1998), The ACE Magnetic Fields Experiment, *Space Sci. Rev.*, *86*, 613–631.

Song, P., G. Le, and C. T. Russell (1994), Observational differences between flux transfer events and surface waves at the magnetopause, *J. Geophys. Res.*, *99*(A2), 2309–2320.

Southwood, D. J., C. J. Farrugia, and M. A. Saunders (1988), What are flux transfer events?, *Planet. Space Sci.*, *36*, 503–508.

Thomsen, M. F., J. A. Stansberry, S. J. Bame, S. A. Fuselier, and J. T. Gosling (1987), Ion and electron velocity distributions within flux transfer events, *J. Geophys. Res.*, *92*(A11), 12127–12136.

Tsyganenko, N. A. (2002a), A model of the near magnetosphere with a dawn-dusk asymmetry 1. Mathematical structure, *J. Geophys. Res.*, *107*(A8), 1179, doi:10.1029/2001JA000219.

Tsyganenko, N. A. (2002b), A model of the near magnetosphere with a dawn-dusk asymmetry 2. Parameterization and fitting to observations, *J. Geophys. Res.*, *107*(A8), 1176, doi:10.1029/2001JA000220.

Wang, J., M. W. Dunlop, Z. Y. Pu, X. Z. Zhou, X. G. Zhang, Y. Wei, S. Y. Fu, C. J. Xiao, A. Fazakerley, H. Laakso, M. G. G. T. Taylor, Y. Bogdanova, F. Pitout, J. Davies, Q. G. Zong, C. Shen, Z. X. Liu, C. Carr, C. Perry, H. Rème, I. Dandouras, P. Escoubet, and C. J. Owen (2007), TC1 and Cluster observation of an FTE on 4 January 2005: A close conjunction, *Geophys. Res. Lett.*, *34*, L03106, doi:10.1029/2006GL028241.

Wild, J. A., S. W. H. Cowley, J. A. Davies, H. Khan, M. Lester, S. E. Milan, G. Provan, T. K. Yeoman, A. Balogh, M. W. Dunlop, K.-H. Fornacon, and E. Georgescu (2001), First simultaneous observations of flux transfer events at the high-latitude magnetopause by the Cluster spacecraft and pulsed radar signatures in the conjugate ionosphere by the CUTLASS and EISCAT radars, *Ann. Geophys.*, *19*, 1491–1508.

Wild, J. A., S. E. Milan, S. W. H. Cowley, M. W. Dunlop, C. J. Owen, J. M. Bosqued, M. G. G. T. Taylor, J. A. Davies, M. Lester, N. Sato, A. S. Yukimatu, A. N. Fazakerley, A. Balogh, and H. Rème (2003), Coordinated interhemispheric SuperDARN radar observations of the ionospheric response to flux transfer events observed by the Cluster spacecraft at the high-latitude magnetopause, *Ann. Geophys.*, *21*, 1807–1826.

Wild, J. A., S. E. Milan, J. A. Davies, M. W. Dunlop, D. W. Wright, C. M. Carr, A. Balogh, H. Rème, A. N. Fazakerley, and A. Marchaudon (2007), On the location of dayside magnetic reconnection during an interval of duskward oriented IMF, *Ann. Geophys.*, *25*, 219–238.

Zhang, Q.-H., R. Y. Liu, M. W. Dunlop, J. Y. Huang, H. Q. Hu, M. Lester, Y. H. Liu, Z. J. Hu, Q. Q. Shi, and M. G. G. T. Taylor (2008), Simultaneous tracking of reconnected flux tubes: Cluster and conjugate SuperDARN observations on 1 April 2004, *Ann. Geophys.*, *26*, 1545–1557.

Y. V. Bogdanova, Mullard Space Science Laboratory, University College London, Dorking, Surrey, RH5 6NT, UK.

M. W. Dunlop, M. Lockwood, and I. W. McCrea, SSTD, Rutherford-Appleton Laboratory, Chilton, Didcot, Oxfordshire, OX11 0QX, UK.

D.-S. Han, H.-Q. Hu, Z.-J. Hu, R.-Y. Liu, S.-L. Liu, H.-G. Yang, B.-C. Zhang, and Q.-H. Zhang, Polar Research Institute of China, NO. 451, Jinqiao Road, Pudong, Shanghai, 200136 China. (zhangqinghe@pric.gov.cn)

M. Lester, Department of Physics and Astronomy, University of Leicester, Leicester, UK.

C. Shen, CSSAR, Chinese Academy of Sciences, Beijing 100080, China.